Comput Mech (2005) 35: 182–189
DOI 10.1007/s00466-004-0615-8

ORIGINAL PAPER

X. F. Pan · X. Zhang[1] · M. W. Lu

Meshless Galerkin least-squares method

Received: 15 April 2004 / Accepted: 19 July 2004 / Published online: 1 September 2004

Abstract Collocation method and Galerkin method have been dominant in the existing meshless methods. Galerkin-based meshless methods are computational intensive, whereas collocation-based meshless methods suffer from instability. A new efficient meshless method, meshless Galerkin lest-squares method (MGLS), is proposed in this paper to combine the advantages of Galerkin method and collocation method. The problem domain is divided into two subdomains, the interior domain and boundary domain. Galerkin method is applied in the boundary domain, whereas the least-squares method is applied in the interior domain.The proposed scheme elliminates the posibilities of spurious solutions as that in the least-square method if an incorrect boundary conditions are used. To investigate the accuracy and efficiency of the proposed method, a cantilevered beam and an infinite plate with a central circular hole are analyzed in detail and numerical results are compared with those obtained by Galerkin-based meshless method (GBMM), collocation-based meshless method (CBMM) and meshless weighted least squares method (MWLS). Numerical studies show that the accuracy of the proposed MGLS is much higher than that of CBMM and is close to, even better than, that of GBMM, while the computational cost is much less than that of GBMM.

Keywords Meshless · Meshfree · Least-squares · Galerkin method

1 Introduction

Two methods of discretization, namely collocation method and Galerkin method [1–9], have been dominant in the existing meshless methods. Although Galerkin method possesses several advantages, one of the major difficulties in the implementation of Galerkin-based meshless method (GBMM) is how to evaluate integrals in the weak form. Nodal integration, cell or octree quadrature, and background finite element mesh quadrature [1] have been used. The first of these is the fastest, but appears to suffer from instability and several stabilization schemes have been developed [10–11]. The second and third have the disadvantage that the resulting method is not truly meshless. In GBMM, derivatives in domain integrals are lowered by using the divergence theorem to establish the weak form. The inaccuracy in integration will result in significant error in the solution. However, the shape functions in meshless method are very complex. Delicate background cells and a large number of quadrature points must generally be employed to integrate the weak form as accurate as possible. As a consequence, the GBMM is much more expensive than FEM.

In contrast, collocation-based meshless methods (CBMM) are truly meshless and very efficient [4–9]. However, equilibrium conditions are satisfied only at nodes within the problem domain but not at the boundary nodes. Hence significant error can be resulted. These methods also suffer from instability. For instance, the collocation methods based on the radial basis function (RBF) have attracted a great deal of attention in recent decades. The traditional domain-type Kansa method has less accuracy in the surface-adjacent region since the governing equations are not satisfied there. By using the Green second identity, Chen [7] developed a modified Kansa method (MKM) to meet equilibrium conditions both on boundary and domain nodes, and the solution accuracy of the boundary region is thus greatly improved. In addition, the MKM holds symmetricity for the self-adjoint equations. On the other hand, for boundary-type RBF-based meshfree methods, Chen [8] and Chen and Hon [9] introduce the boundary knot method (BKM), which is truly meshfree, spectral convergent, symmetric, integration-free (collocation), and very easy to learn and implement. However, all

X. Zhang
Department of Engieering Mechanics, Tsinghnua University, Beijing 100084, P. R. China
E-mail: xzhang@tsinghua.edu.cn

these collocation RBF techniques still encounter ill-conditioning full matrix, and thus can not be effectively applied to practical large-size problems.

The Least-squares method has been successfully used in the finite element method, and several least-squares finite element method (LSFEM) have been established [12–13]. In the least-squares method, integration is only used to average the residual of the governing equations. The solution accuracy in the least-squares method is less sensitive to the integration accuracy than in the Galerkin method [15]. A new efficient meshless method, meshless weighted least-square (MWLS) method, was proposed in [14] based on the weighted least-squares method. Unlike Galerkin method, the Euler equations which obtained from the least-squares variational principle no longer give the original differential equations, but give higher order derivatives of these equations. This introduces the possibility of spurious solutions if incorrect boundary conditions are used [12].

In this paper, MGLS method is proposed by combining the advantages of Galerkin method and collocation method to overcome the disadvantages of MWLS. The problem domain is divided into two subdomains: the boundary domain and interior domain. The Galerkin method is applied in the boundary domain, whereas the least-squares method is applied in the interior domain. The moving least-square (MLS) approximation is used to construct the trial functions in both boundary domain and interior domain. The Euler equations obtained from the proposed method give the original differential equations in the boundary domain, while give higher order derivatives of these equations in the interior domain. No boundary conditions are applied on the boundary of the interior domain, so the proposed method eliminates the possibility of spurious solutions, while preserves the efficiency of collocation methods.

Compared with CBMM and GBMM, the new method possesses several advantages. It is much more accurate and stable than CBMM, and is much more efficient than GBMM. Same as all collocation methods, MGLS requires the calculation of second order derivatives in the interior domain that would typically not required in GBMM.

2 Moving least-square approximation

In MLS approximation, the function u(x) is approximated in the domain by $\widehat{u}(\mathbf{x})$, namely

$$u(\mathbf{x}) \approx \widehat{u}(\mathbf{x}) = \sum_{i=1}^{m} p_i(\mathbf{x}) \cdot a_i(\mathbf{x}) = p^{\mathrm{T}}(\mathbf{x}) \cdot \mathbf{a}(\mathbf{x}) \ , \qquad (1)$$

where m is the number of terms in the basis, $p_i(\mathbf{x})$ are monomial basis functions and $a_i(\mathbf{x})$ are their coefficients, which are functions of the spatial coordinates $\mathbf{x}$. For 2D problems, examples of commonly used basis are the linear basis $p^T = [1, x, y]$ and the quadratic basis $p^T = [1, x, y, x^2, xy, y^2]$. It is also possible to use other functions, such as singular functions, in a basis. The coefficients $a_i(\mathbf{x})$ are obtained by minimizing the quadratic functional $J(\mathbf{x})$ given by

$$J(\mathbf{x}) = \sum_{I=1}^{k} w_I(\mathbf{x}) \cdot \left[\sum_{i=1}^{m} p_i(\mathbf{x}_I) \cdot a_i(\mathbf{x}) - u_I \right]^2 \ , \qquad (2)$$

where $u_I = u(\mathbf{x}_I)$ is the nodal value of $u(\mathbf{x})$ at node $\mathbf{x}_I, w_I(\mathbf{x}) = w(\mathbf{x} - \mathbf{x}_I)$ is a non-negative weight function with compact support associated with node $\mathbf{x}_I$ and maximum at node $\mathbf{x}_I$. Moreover, k is the total number of nodes at which the weight function $w_I(\mathbf{x})$ does not vanish. Minimizing the functional $J(\mathbf{x})$ results in

$$\mathbf{A}(\mathbf{x}) \cdot \mathbf{a}(\mathbf{x}) = \mathbf{B}(\mathbf{x}) \cdot \mathbf{u} \ , \qquad (3)$$

where

$$\mathbf{A}(\mathbf{x}) = \sum_{I=1}^{k} w_I(\mathbf{x}) \mathbf{p}(\mathbf{x}_I) \mathbf{p}^{\mathrm{T}}(\mathbf{x}_I) \ , \qquad (4)$$

$$\mathbf{B}(\mathbf{x}) = [w_1(\mathbf{x})\mathbf{p}(\mathbf{x}_1) \ w_2(\mathbf{x})\mathbf{p}(\mathbf{x}_2), \ldots, w_k(\mathbf{x})\mathbf{p}(\mathbf{x}_k)] \ , \qquad (5)$$

$$\mathbf{u} = [u_1, u_2, \ldots, u_k]^{\mathrm{T}} \qquad (6)$$

Solve (3) for $\mathbf{a}(\mathbf{x})$ at $\mathbf{x}$, and then substitute $\mathbf{a}(\mathbf{x})$ into (1), the MLS approximation function is finally obtained as

$$\widehat{u}(\mathbf{x}) = \boldsymbol{\phi}^{\mathrm{T}}(\mathbf{x})\mathbf{u} \ , \qquad (7)$$

or in indicial notation

$$\widehat{u}(\mathbf{x}) = \boldsymbol{\phi}_I(\mathbf{x}) u_I, I = 1, 2, \ldots, k \qquad (8)$$

where the index $\boldsymbol{I}$ is summed over its range, which depends on the context. The shape function $\boldsymbol{\phi}(\mathbf{x})$ is given by

$$\boldsymbol{\phi}^{\mathbf{T}}(\mathbf{x}) = \mathbf{p}^{\mathbf{T}}\mathbf{x} \cdot \mathbf{A}^{-1}(\mathbf{x}) \cdot \mathbf{B}(\mathbf{x}). \qquad (9)$$

In MLS approximation, the local values of the approximation function $\widehat{u}(x)$ do not fit the nodal unknown values $u_I(\mathbf{I} = 1, 2, \ldots, N)$, namely, $u_I = u(\mathbf{x}_I) \neq (\mathbf{x}_I)$. Indeed $\widehat{u}(\mathbf{x})$ is the true approximation for which we shall seek the satisfaction of the differential equation and boundary conditions and u_I are simply the unknown parameters sought.

If the weight function, $w_I(\mathbf{x})$, together with its first l derivatives are continuous, the MLS shape function $\boldsymbol{\phi}(\mathbf{x})$ and its first l derivatives are also continuous. Hence, the weight function plays an important role in the performance of MLS approximation. The cubic spline function

$$w_I(r) = \begin{cases} \frac{2}{3} - 4r^2 + 4r^3 & r \frac{1}{2} \\ \frac{4}{3} - 4r + 4r^2 - \frac{4}{3}r^3 & \frac{1}{2} < r 1 \\ 0 & r > 1 \end{cases} \ , \qquad (10)$$

is used in this paper, where $r = ||\mathbf{x}_I - \mathbf{x}||/d_{\max}, d_{\max}$ is the radius of the domain of definition of point **x.** In this paper, $d_{\max}$ is determined by $scale \times s[k]$, where $s[k]$ is the distance between point $\mathbf{x}$ and its $k - th$ closest nodes.

3 Meshless weighted least-squares method

Least-squares variational principles are applicable to any set of differential equations including linear and nonlinear equations. In this paper, the 2D static elasticity problem is taken as an example. However, the scheme proposed in this paper can be extended to any problems.

Consider the 2D static elasticity problem

$$\begin{aligned} &\sigma_{ij,j}+\bar{f}_i=0 \quad \text{in} \quad \Omega \\ &\sigma_{ij}n_j-\bar{t}_i=0 \quad \text{on} \quad \Gamma_t \\ &u_i-\bar{u}_i=0 \quad \text{on} \quad \Gamma_u \end{aligned} \tag{11}$$

where Γ_u is the prescribed displacement boundary and Γ_t is the prescribe traction boundary. $\bar{f}_i, \bar{u}_i$ and $\bar{t}_i$ are prescribed functions defined in the domain Ω, displacement boundary Γ_u and traction boundary Γ_t, respectively. n_j are the direction cosines of the outward normal to the boundary Γ_t. In (11), indices repeated twice in a term are summed over their range.

Several methods are available for solving (11). However, Galerkin and Collocation are the most frequently used ones in the existing meshless methods. In this paper, the least-squares method [12] [13] is used, namely

$$\begin{aligned} \delta\Pi=&\int_\Omega \delta\sigma_{ik,k}(\sigma_{ij,j}+\bar{f}_i)\mathrm{d}\Omega+\int_{\Gamma_u}\lambda_u\delta u_i(u_i-aru_i)\mathrm{d}\Gamma \\ &+\int_{\Gamma_t}\lambda_t\delta\sigma_{ik}n_k(\sigma_{ij}n_j-\bar{t}_i)\mathrm{d}\Gamma \end{aligned} \tag{12}$$

where λ_u and λ_t are the penalty functions for imposing the boundary conditions. Like Galerkin method, integrations are involved in (12), therefore, significant computational effort is required. In GBMM, the functional Π is the total potential energy of the system and must be integrated as accurate as possible. However, in the present method, the functional Π is the weighted square of the residual of the equilibrium equation and boundary condition. Therefore, the integration is only used to average the residual of the governing equations, and the solution accuracy in the least-squares method is much less sensitive to the integration accuracy than in the Galerkin method [15]. To avoid involving any integration, an alternative discrete formulation of (12) is used, namely

$$\begin{aligned} \delta\Pi=&\sum_{s=1}^{N}\delta\sigma_{ik,k}(\sigma_{ij,j}+\bar{f}_i)\big|_{x=x_s}+\sum_{s=1}^{N_u}\lambda_u\delta u_i(u_i-\bar{u}_i)\big|_{x=x_s} \\ &+\sum_{s=1}^{N_t}\lambda_t\delta\sigma_{ik}n_k(\sigma_{ij}n_j-\bar{t}_i)\big|_{\mathbf{x}=\mathbf{x}_s} \\ =&0 \ , \end{aligned} \tag{13}$$

where N is the total number of nodes, N_u is the total number of nodes located on the boundary Γ_u and N_t is the total number of nodes located on the boundary Γ_t. Substitution of the MLS approximation (8) into (13) results in

$$\begin{aligned} \delta\Pi=&\delta u_{iI}\left[\sum_{s=1}^{N}\phi_{I,mk}D_{lkim}D_{ljpq}\phi_{J,qj}u_{pJ}+\sum_{s=1}^{N_u}\lambda_u\phi_I\phi_J u_{iJ}\right. \\ &\left.+\sum_{s=1}^{N_t}\lambda_t\phi_{I,m}n_kD_{lkim}D_{ljpq}\phi_{J,q}n_ju_{pJ}\right]_{x=x_s} \\ &+\delta u_{iI}\left[\sum_{s=1}^{N}\phi_{I,mk}D_{lkim}\bar{f}_l-\sum_{s=1}^{N_u}\lambda_u\phi_I\bar{u}_i\right. \\ &\left.-\sum_{s=1}^{N_t}\lambda_t\phi_{I,m}n_kD_{lkim}\bar{t}_i\right]_{x=x_s}=0 \ . \end{aligned} \tag{14}$$

where u_{iI} denotes the nodal displacement u_i of node I. Rewriting (14) in matrix form by using Voigt rule and invoking the arbitrariness of the virtual displacements give

$$\mathbf{KU}=\mathbf{P} \ , \tag{15}$$

where

$$\mathbf{K}=\sum_{i=1}^{N}\mathbf{H}^{\mathrm{T}}\mathbf{H}+\sum_{j=1}^{N_u}\lambda_u\mathbf{N}^{\mathrm{T}}\mathbf{N}+\sum_{k=1}^{N_t}\lambda_t\mathbf{Q}^{\mathrm{T}}\mathbf{Q} \ , \tag{16}$$

$$\mathbf{P}=-\sum_{i=1}^{N}\mathbf{H}^{\mathrm{T}}\bar{\mathbf{f}}+\sum_{j=1}^{N_u}\lambda_u\mathbf{N}^{\mathrm{T}}\mathbf{U}+\sum_{k=1}^{N_t}\lambda_t\mathbf{Q}^{\mathrm{T}}\bar{\mathbf{t}} \ , \tag{17}$$

$$\mathbf{U}=[u_1,u_2,\ldots,u_N]^T. \tag{18}$$

In (16) and (17),

$$N=\begin{bmatrix}\varphi_1 & 0 & \varphi_2 & 0 & \cdots & \varphi_N & 0\\ 0 & \varphi_1 & 0 & \varphi_2 & \cdots & 0 & \varphi_N\end{bmatrix} \ , \tag{19}$$

$$\mathbf{H}=E'\begin{bmatrix}\frac{\partial^2\varphi_1}{\partial x^2}+\frac{1-v}{2}\frac{\partial^2\varphi_1}{\partial y^2} & \frac{1+v}{2}\frac{\partial^2\varphi_1}{\partial x\partial y} & \cdots & \frac{\partial^2\varphi_N}{\partial x^2}+\frac{1-v}{2}\frac{\partial^2\varphi_N}{\partial y^2} & \frac{1+v}{2}\frac{\partial^2\varphi_N}{\partial x\partial y}\\ \frac{1+v}{2}\frac{\partial^2\varphi_1}{\partial x\partial y} & \frac{\partial^2\varphi_1}{\partial y^2}+\frac{1-v}{2}\frac{\partial^2\varphi_1}{\partial x^2} & \cdots & \frac{1+v}{2}\frac{\partial^2\varphi_N}{\partial x\partial y} & \frac{\partial^2\varphi_N}{\partial y^2}+\frac{1-v}{2}\frac{\partial^2\varphi_N}{\partial x^2}\end{bmatrix} \ , \tag{20}$$

$$\mathbf{Q}=E'\times\begin{bmatrix}l\frac{\partial\varphi_1}{\partial x}+m\frac{1-v}{2}\frac{\partial\varphi_1}{\partial y} & lv\frac{\partial\varphi_1}{\partial y}+m\frac{1-v}{2}\frac{\partial\varphi_1}{\partial x} & \cdots & l\frac{\partial\varphi_N}{\partial x}+m\frac{1-v}{2}\frac{\partial\varphi_N}{\partial y} & lv\frac{\partial\varphi_N}{\partial y}+m\frac{1-v}{2}\frac{\partial\varphi_N}{\partial x}\\ mv\frac{\partial\varphi_1}{\partial x}+l\frac{1-v}{2}\frac{\partial\varphi_1}{\partial y} & m\frac{\partial\varphi_1}{\partial y}+l\frac{1-v}{2}\frac{\partial\varphi_1}{\partial x} & \cdots & mv\frac{\partial\varphi_N}{\partial x}+l\frac{1-v}{2}\frac{\partial\varphi_N}{\partial y} & m\frac{\partial\varphi_N}{\partial y}+l\frac{1-v}{2}\frac{\partial\varphi_N}{\partial x}\end{bmatrix} \ , \tag{21}$$

where $E' = E/(1-\nu^2)$. It can be observed from (19) and (21) that the entries of matrix **N** and **Q** are of different order of magnitude, so that the penalty functions λ_u and λ_t should also be of different order of magnitude. In this paper, $\lambda_t = 10^5, \lambda_u = \lambda_t[E/(1-\nu^2)]^2$. Because no integrals are required in the calculation of the coefficient matrix **K**, the meshless weighted least square method (MWLS) is much more efficient than Galerkin method. The coefficient matrix **K** is symmetric and positive.

4 Meshless Galerkin least-squares method

Unlike Galerkin method, the Euler equations which obtained from the least-squares variational principle (12) no longer give the original differential equations (11), but give higher order derivatives of these equations. This introduces the possibility of spurious solutions if incorrect boundary conditions are used [12], which will be shown clearly in the numerical results presented in Sect. 5.

To overcome this drawback, a MGLS is developed. The domain Ω is divided into two subdomains, the interior domain Ω_1 and boundary domain Ω_2, as shown in Fig. 1. Galerkin method is applied in the boundary domain Ω_2, whereas the least-squares method is applied in the interior domain Ω_1. Hence, we have

$$\delta\bar{\Pi} = -\lambda\int_{\Omega_1}\delta\sigma_{ik,k}(\sigma_{ij,j}+\bar{f}_i)\mathrm{d}\Omega + \int_{\Omega_2}\delta u_i(\sigma_{ij,j}+\bar{f}_i)\mathrm{d}\Omega - \int_{\Gamma_t}\delta u_i(\sigma_{ij}n_j-\bar{t}_i)\mathrm{d}\Gamma = 0 \tag{22}$$

where Γ_t is the part of boundary Γ_2 on which the traction is prescribed. λ is a weight that can be chosen as $1/E$ to make every terms in (22) in the same order.

Integrating the second term by parts, equation (22) can be rewritten as

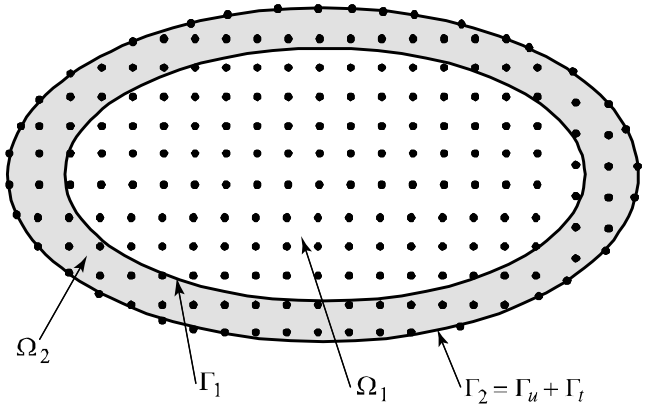

Fig. 1 The boundary domain and interior domain

$$\delta\bar{\Pi} = -\lambda\int_{\Omega_1}\delta\sigma_{ik,k}(\sigma_{ij,j}+\bar{f}_i)\mathrm{d}\Omega - \int_{\Omega_2}\delta\varepsilon_{ij}\sigma_{ij}\mathrm{d}\Omega + \int_{\Omega_2}\delta u_i\bar{f}_i\mathrm{d}\Omega + \int_{\Gamma_t}\delta u_i\bar{t}_i\mathrm{d}\Gamma + \int_{\Gamma_1}\delta u_i\sigma_{ij}n_j\mathrm{d}\Gamma = 0 \tag{23}$$

Belytschko et al.[16] coupled EFG to finite elements based on a blending approach where blending functions are used to combine the finite element and meshless approximations on the interface zone. In the present MGLS method, the domain Ω is divided into two subdomains only for the purpose of evaluation of the functional. From the physical point of view, the domain Ω is not divided into subdomains, and the trail function and its derivatives are continuous across the boundary Γ_1. Consequently, no special scheme is requried to couple the the interior domain Ω_1 and boundary domain Ω_2.

The integration in the first term of (23) is used to average the residual of the equilibrium equations in the interior domain Ω_1, which can be replaced by its discrete form because the solution accuracy in the least-squares method is much less sensitive to the integration accuracy than in the Galerkin method. We have

$$\delta\bar{\Pi} = -\lambda\sum_{s=1}^{N_1}\delta\sigma_{ik,k}(\sigma_{ij,j}+\bar{f}_i)|_{\mathbf{x}=\mathbf{x}_s} - \int_{\Omega_2}\delta\varepsilon_{ij}\sigma_{ij}\mathrm{d}\Omega + \int_{\Omega_2}\delta u_i\bar{f}_i\mathrm{d}\Omega + \int_{\Gamma_t}\delta u_i\bar{t}_i\mathrm{d}\Gamma + \int_{\Gamma_1}\delta u_i\sigma_{ij}n_j\mathrm{d}\Gamma = 0 \tag{24}$$

where N_1 is the total number of nodes located in the interior domain Ω_1, namely $\mathbf{x}_s \in \Omega_1$, $s = 1, 2, \ldots, N_1$. Substituting MLS approximation (8) into (24) and invoking the arbitrariness of the virtual nodal displacements δu_{iI}, we get

$$\mathbf{KU} = \mathbf{P} \tag{25}$$

where

$$\mathbf{K} = \int_{\Omega_1}\mathbf{B}^{\mathrm{T}}\mathbf{DB}\mathrm{d}\Omega - \int_{\Gamma_{12}}\mathbf{N}^{\mathrm{T}}\mathbf{Q}\mathrm{d}\Gamma + \sum_{s=1}^{N_2}\lambda\mathbf{H}^{\mathrm{T}}\mathbf{H} \tag{26}$$

$$\mathbf{P} = \int_{\Omega_1}\mathbf{N}^{\mathrm{T}}\bar{\mathbf{f}}\mathrm{d}\Omega + \int_{\Gamma_t}\mathbf{N}^{\mathrm{T}}\bar{\mathbf{t}}\mathrm{d}\Gamma - \sum_{s=1}^{N_2}\mathbf{H}^{\mathrm{T}}\bar{\mathbf{f}} \tag{27}$$

in which **N**, **H** and **Q** are given by (19)–(21), and

$$\mathbf{B} = \begin{bmatrix} \frac{\partial\varphi_1}{\partial x} & 0 & \cdots & \frac{\partial\varphi_N}{\partial x} & 0 \\ 0 & \frac{\partial\varphi_1}{\partial y} & \cdots & 0 & \frac{\partial\varphi_N}{\partial y} \\ \frac{\partial\varphi_1}{\partial y} & \frac{\partial\varphi_1}{\partial x} & \cdots & \frac{\partial\varphi_N}{\partial y} & \frac{\partial\varphi_N}{\partial x} \end{bmatrix},$$

$$\mathbf{D} = \frac{E_0}{1-\nu_0^2}\begin{bmatrix} 1 & \nu_0 & 0 \\ \nu_0 & 1 & 0 \\ 0 & 0 & \frac{1-\nu_0}{2} \end{bmatrix} \text{ (for plane stress)}$$

In the present method, integrals are involved only in the boundary domain Ω_2, which is usually a thin layer of domain and is much smaller than the interior domain Ω_1. Consequently, the computational effort required is much less than that required for GBMM, while the imposition of boundary conditions is the same as that in GBMM. Numerical studies show that the present method is stable.

The moving least-square (MLS) approximation is used to construct the trial functions in both boundary domain and interior domain. Consequently, a appropriate scheme must be used to enforce displacement (Dirichlet) boundary conditions. In the present paper, the penalty method is used. An alternative scheme is to use FEM interpolants in the boundary, which automatically satisfy displacement type boundary conditions [16].

Note that the least-square method is used in the interior domain, whereas the Galerkin method is used in the boundary domain. Consequently, the Euler equations obtained from the present MGLS method give the original differential equations in the boundary domain, while give higher order derivatives of these equations in the interior domain. No boundary conditions are applied on the boundary of the interior domain, so the proposed method eliminates the possibility of spurious solutions.

5 Numerical examples

In this section, two numerical results are presented to evaluate the accuracy and efficiency of the present MGLS approach. To evaluate the accuracy of each method, the following error norms are used

$$L_u = \frac{\sqrt{\int_\Omega (\hat{\mathbf{u}} - \mathbf{u})^T \cdot (\hat{\mathbf{u}} - \mathbf{u}) \mathrm{d}\Omega}}{\sqrt{\int_\Omega \mathbf{u}^T \cdot \mathbf{u} \mathrm{d}\Omega}} \times 100\%$$

$$L_\sigma = \frac{\sqrt{\int_\Omega (\hat{\boldsymbol{\sigma}} - \boldsymbol{\sigma})^T \cdot (\hat{\boldsymbol{\sigma}} - \boldsymbol{\sigma}) \mathrm{d}\Omega}}{\sqrt{\int_\Omega \boldsymbol{\sigma}^T \cdot \boldsymbol{\sigma} \mathrm{d}\Omega}} \times 100\%$$

where $\hat{\mathbf{u}}$ and $\mathbf{u}$ are the approximation and exact value of displacement at point $\mathbf{x}$, $\hat{\boldsymbol{\sigma}}$ and $\boldsymbol{\sigma}$ are the approximation and exact value of stress at point x.

5.1 Cantilevered beam

The cantilevered beam subjected to end load as shown in Fig. 2(a) is analyzed with dimensionless elastic modulus $E = 1.0 \times 10^4$, $P = 6$, $D = 2$ and $L = 12.5 \times 17$ regular nodes, as shown in Fig. 2(b), are used in this analysis. The Poisson's ratio is chosen as $v = \frac{1}{3}$ and $v = 0.499999$, respectively. To investigate the effects of boundary conditions, two cases are analyzed. In the first case, the left edge of the beam is fixed, while in the second case the exact analytical displacement is prescribed on the left edge of the beam. The upper and lower edges of the beam are traction-free.

Table 1 Error norm obtained by using different methods for the cantilevered beam

	$v = 0.333333$			$v = 0.499999$		
	scale	$L_u(\%)$	$L_\sigma(\%)$	*Scale*	$L_u(\%)$	$L_\sigma(\%)$
MWLS	1.2	4.221	9.201	1.2	53.70	54.94
	1.5	18.16	38.85	1.5	69.46	75.20
	2.0	10.19	14.52	2.0	62.08	63.71
CBMM	1.2	146.1	150.2	1.2	145.6	149.3
	1.5	287.6	468.8	1.5	227.8	421.5
	2.0	8.187	20.16	2.0	29.62	34.13
GBMM	1.2	0.085	6.669	1.2	0.214	7.414
	1.5	0.582	8.652	1.5	0.868	9.328
	2.0	1.035	10.53	2.0	1.424	11.09
MGLS	1.2	2.186	5.170	1.2	2.622	6.329
	1.5	1.048	4.223	1.5	1.410	5.913
	2.0	4.858	10.06	2.0	6.055	11.01

Table 1 compares the error norms obtained by using different methods with different value of parameter *scale*. It can be seen that the parameter *scale* has significant effects on the results. As it is well known, CBMM is unstable. It also indicates that the CBMM and MWLS are locked for the nearly incompressible material, while the MGLS and GBMM still give results with satisfactory accuracy. This example shows that MGLS appears to be stable and its accuracy is close to that of GBMM.

Figure 3 compares the stresses σ_{xx} at stations along the upper surface obtained by the different methods for the first case, whereas figure 4 compares those for the second case. These results show that MWLS leads to spurious solutions for the first case in which the left edge of the beam is fixed so the boundary condition is in contradiction to the analytical solution. However, MGLS gives correct solution in both cases. Parameters used in the construction of MLS approximation are assumed to be $scale = 1.2$ and $k = 12$. Poisson's ratio $v = 1/3$.

Figure 5 compares the displacement and stress convergence rate of MWLS, CBMM, WGLS and GBMM. The mesh size h in these figures is defined as the distance

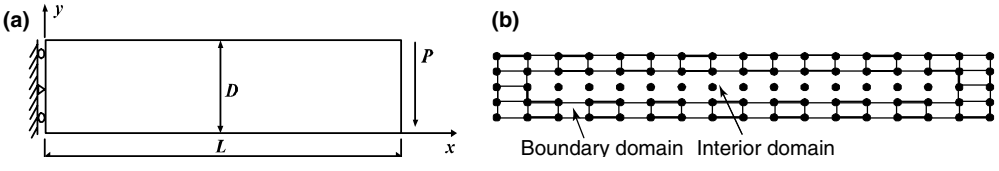

Fig. 2 Cantilevered beam and its nodal arrangement

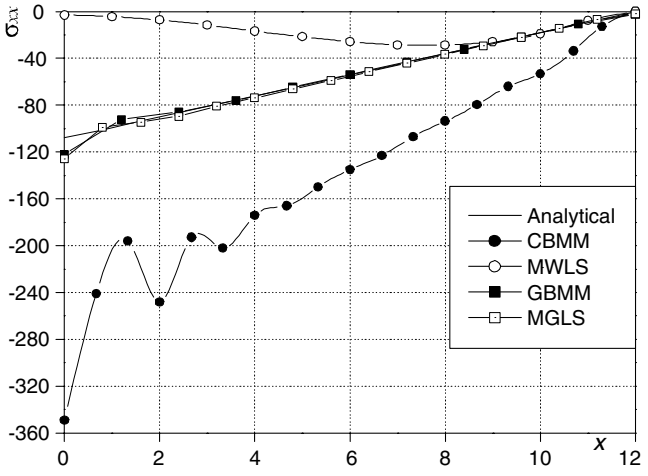

Fig. 3 Stress σ_{xx} at stations along the upper surface of the beam for the first case

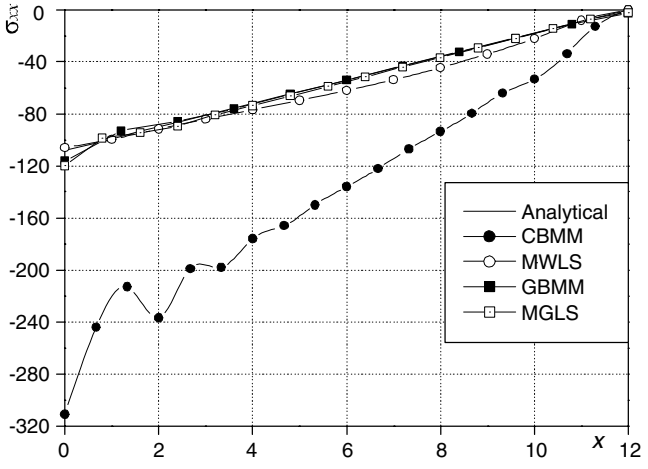

Fig. 4 Stress σ_{xx} at stations along the upper surface of the beam for the second case

in y direction between two neighboring nodes with same x coordinate. *scale* is set to 1.2 and Poison's ratio $v = 1/3$ in this computation.

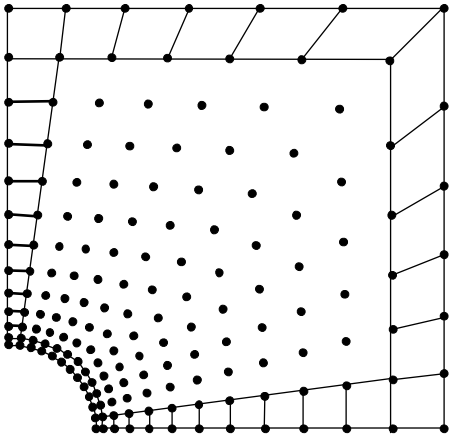

Fig. 6 Infinite plate discretized with 169 nodes

5.2 Infinite plate with a central circular hole

Consider the problem of an infinite plate with a central circular hole of radius a. The plate is subject to a uniform tension, σ_0, in the x direction at infinity. Due to symmetry, only the upper right quadrant of the plate is modelled and the overall dimension of the quadrant is $5a \times 5a$. A plane stress state is assumed with dimensionless elastic modulus $E = 1 \times 10^3$. In this analysis, σ_0 is assumed to be 1. The Poisson's ratio is chosen as $v = 1/3$ and $v = 0.499999$, respectively. Two cases are analyzed. In the first case, the symmetric boundary condition is used, namely, all points on the left edge of the plate are fixed in the horizontal direction and free in the vertical direction whereas all points on the bottom edge are free in the horizontal direction and fixed in the vertical direction. In the second case, the exact analytical displacements are imposed on the left and bottom edges. In both cases, the exact analytical tractions are prescribed at the right and upper boundary, and the periphery of the circular hole is traction-free. Nodal arrangement and the boundary domain are shown in Fig. 6.

Figure 7 compares the stresses σ_{xx} at stations along the left edge of the plate obtained by the different methods for the first case, whereas Fig. 8 compares those for the second case. These results also show that

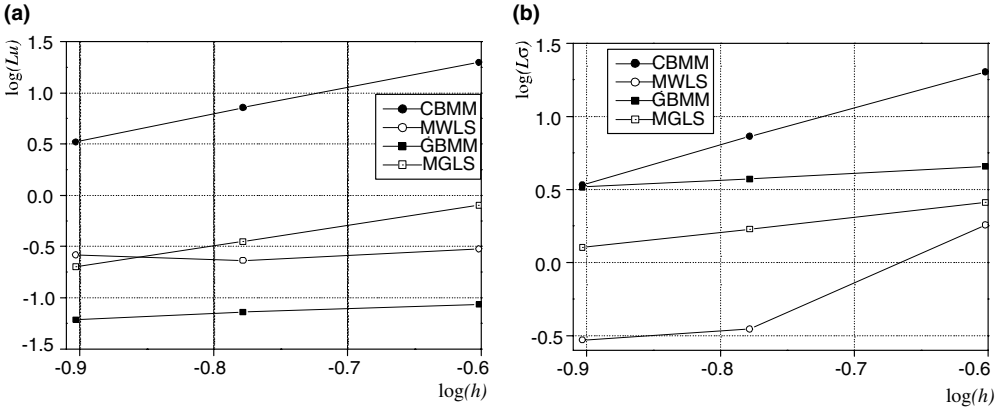

Fig. 5 Displacement convergence rate and stress convergence rate

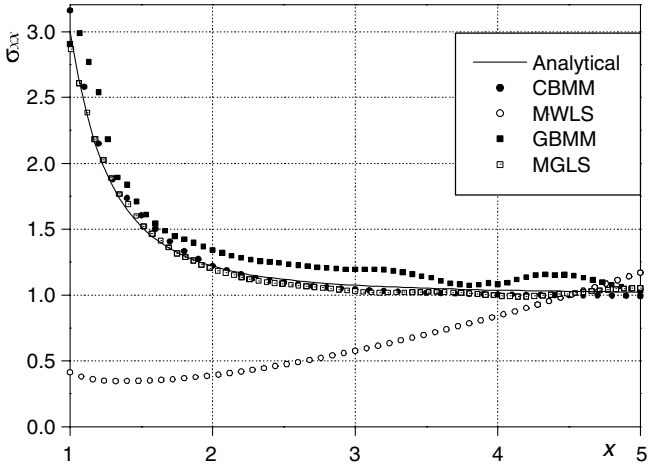

Fig. 7 Stress σ_{xx} at the stations along the left edge of the plate for the first case

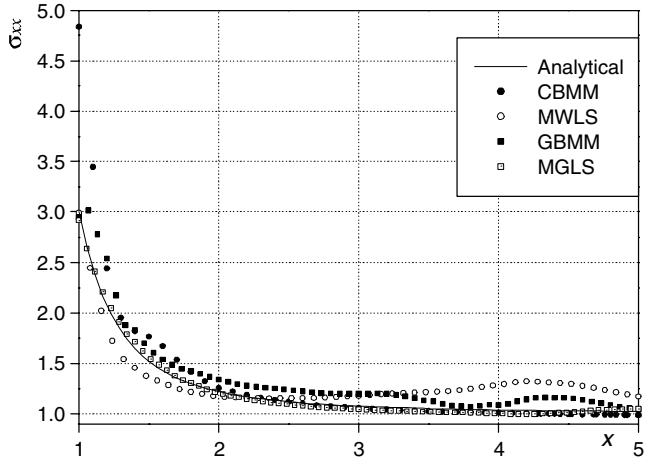

Fig. 8 Stress σ_{xx} at the stations along the left edge of the plate for the second case

MWLS leads to spurious solutions for the first case in which the prescribed displacement boundary conditions are in contradiction to the analytical solution. However, MGLS gives correct solution in both cases. Parameters

Table 2 Error norm obtained by using different methods for the first case

	$v = 0.333333$			$v = 0.499999$		
	scale	$L_u(\%)$	$L_\sigma(\%)$	*Scale*	$L_u(\%)$	$L_\sigma(\%)$
MWLS	1.2	72.75	48.16	1.2	19.58	31.40
	1.5	70.56	43.67	1.5	13.02	20.03
	2.0	65.36	37.65	2.0	3.105	7.032
CBMM	1.2	2.035	2.941	1.2	2.231	12.54
	1.5	4.333	4.834	1.5	6.850	55.30
	2.0	14.70	21.86	2.0	4.422	18.71
GBMM	1.2	0.716	6.248	1.2	0.659	6.527
	1.5	1.303	8.834	1.5	0.932	9.173
	2.0	3.058	11.28	2.0	2.093	11.55
MGLS	1.2	2.233	3.167	1.2	1.876	3.627
	1.5	2.883	5.204	1.5	1.612	5.299
	2.0	2.544	8.041	2.0	2.106	7.411

Table 3 Error norm obtained by using different methods for the second case

	$v = 0.333333$			$v = 0.499999$		
	scale	$L_u(\%)$	$L_\sigma(\%)$	*Scale*	$L_u(\%)$	$L_\sigma(\%)$
MWLS	1.2	12.24	18.46	1.2	73.68	50.21
	1.5	7.685	11.41	1.5	71.90	46.32
	2.0	2.934	34.68	2.0	66.83	38.42
CBMM	1.2	0.575	6.163	1.2	2.384	3.774
	1.5	0.918	8.757	1.5	3.248	4.659
	2.0	2.059	11.06	2.0	53.73	70.33
GBMM	1.2	0.575	6.163	1.2	0.700	6.595
	1.5	0.918	8.757	1.5	1.283	9.218
	2.0	2.059	11.06	2.0	2.939	11.72
MGLS	1.2	1.284	2.702	1.2	2.587	4.045
	1.5	1.461	4.685	1.5	2.080	5.730
	2.0	1.996	6.670	2.0	2.694	8.956

used to construct the MLS approximation are assumed to be *scale* = 1.2 and $k = 12$. In both cases Poison's ratio $v = 1/3$

Figures 9 and 10 compare the displacement and stress convergence rates of CBMM, MGLS and GBMM for the first case and second case, respectively. The mesh size

Fig. 9a, b displacement convergence rate and stress convergence rate for the first case

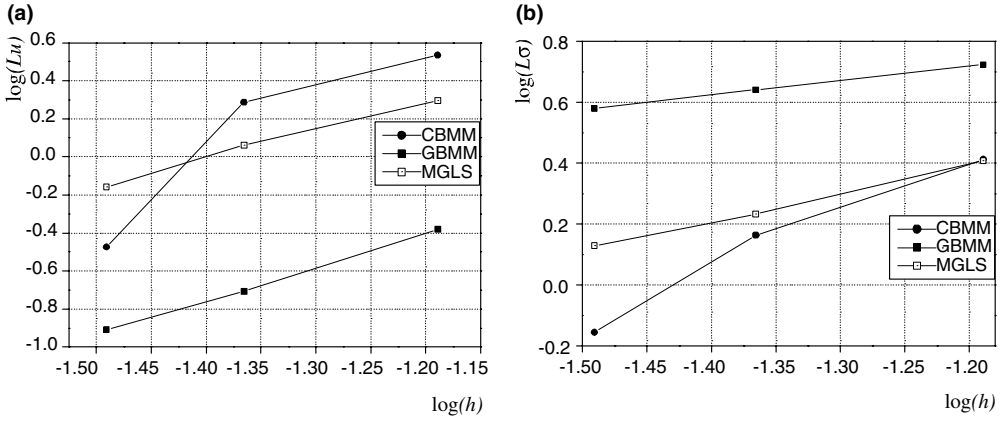

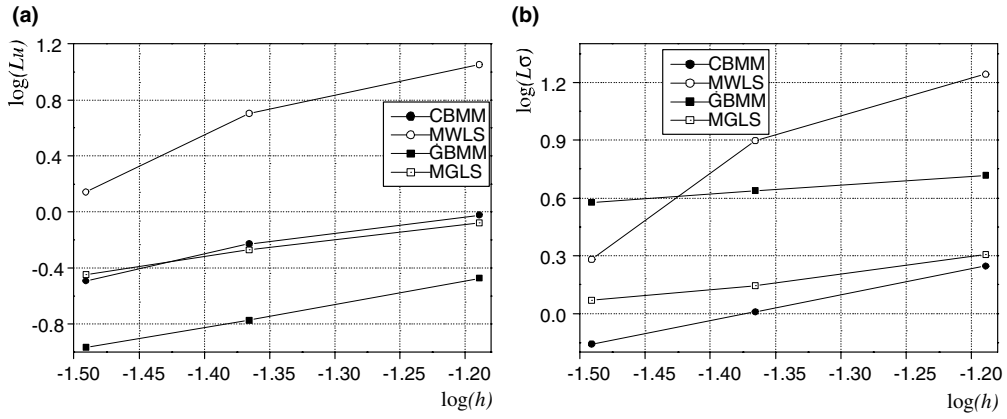

Fig. 10 Displacement convergence rate and stress convergence rate for the second case

h in these figures is defined as the minimal distance in y direction between two neighboring nodes along the left edge. The parameter *scale* is set to 1.2 in this analysis.

Tables 2 and 3 compare the error norms obtained by using different methods with different value of parameter *scale* for the first and second case, respectively. In both cases Poison's ratio $v = 1/3$ which represent a nearly incompressible material. It can be seen that the parameter *scale* has significant effects on the results. This example also shows that MGLS appears to be stable and its accuracy is close to, even better than, that of GBMM.

6. Concluding remarks

Galerkin-based meshless methods are computational intensive, whereas collocation-based meshless methods suffer from instability. Meshless weighted least squares method is very efficient, but it may give spurious solutions if incorrect boundary conditions are used because the Euler equations obtained from the least-squares variational principle no longer give the original differential equations, but give higher order derivatives of these equations. A new efficient meshless method, meshless Galerkin least-squares method, is proposed in this paper. Numerical studies show that the accuracy of the proposed MGLS is much higher than that of CBMM and is very close to, even better than, that of GBMM, while the computational cost is much less than that of GBMM.

Acknowledgements The authors gratefully acknowledge the support of the National Natural Science Foundation of China with grant number 10172052.

Reference

1. Belytschko T, Krongauz Y et al. (1996) Meshless methods: an overview and recent developments. Comput. Meth. Appl. Mech. Eng. 139: 3–47
2. Li S, Liu WK (2002) Meshfree and particle methods and their applications. Appl. Mech. Rev. 55(1): 1–34
3. Wang JG, Liu GR, Lin P (2002) Numerical analysis of Biot's consolidation process by radial point interpolation method. Int. J. Solids Struct. 39(6): 1557–1573
4. Chen JT, Chang MH, Chen KH, et al. (2002) Boundary collocation method for acoustic eigenanalysis of three-dimensional cavities using radial basis function. Comput. Mech. 29(4-5):392–408
5. Jiang PL, Li SQ, Chan CH (2002) Analysis of elliptical waveguides by a meshless collocation method with the Wendland radial basis functions. Microw. Opt. Techn. Let. 32(2): 162–165
6. Kim DW, Kim Y (2003) Point collocation methods using the fast moving least-square reproducing kernel approximation. Int. J. Numer. Meth. Eng. 56(10): 1445–1464
7. Chen W New RBF collocation schemes and kernel RBFs with applications. Lecture Notes Comput. Sci. Eng. 26: 75–86
8. Chen W (2002) Symmetric boundary knot method. Eng. Anal. Bound. Elem. 26(6): 489–494
9. Chen W, Hon YC (2003) Numerical convergence of boundary knot method in the analysis of Helmholtz, modified Helmholtz, and convection-diffusion problems. Comput. Meth. Appl. Mech. Eng. 192: 1859–1875
10. Beissel S, Belytschko T (1996) Nodal integration of the element-free Galerkin method. Comput. Meth. Appl. Mech. Eng. 139: 49–74
11. Nagashima T (1999) Node-by-node meshless approach and its applications to structural analysis. Int. J. Numer. Meth. Eng. 46: 341–385
12. Zienkiewicz OC, Taylor RL (2000) The Finite Element Method (5th edn). Butterworth-Heinemann
13. Jiang BN (1998) The Least-Squares Finite Element Method - Theory and Applications in Computational Fluid Dynamics and Electromagnetics. Springer Berlin Heidelberg
14. Zhang X, Pan XF, et al (2002) Meshless weighted least-square method. Proceedings of Fifth World Congress on Computational Mechanics. Vienna, Austria, July 7–12
15. Park SH, Youn SK (2001) The least-square meshfree method. Int J. Numer. Meth. Eng. 52(9): 997–1012
16. Belytschko T, Organ D, Krongauz Y (1995) A coupled finite element-element-free Galerkin method. Comput. Mech. 17: 186–195